LAWRENCE
LIVERMORE
NATIONAL
LABORATORY

UCRL-JRNL-227093

Emergence of Strong Exchange Interaction in the Actinide Series: The Driving Force for Magnetic Stabilization of Curium

K. Moore, G. van der Laan, D. Haire, M. Wall, A. Schwartz, P. Soderlind

January 5, 2007

Physical Review Letters

Updated October 14, 2003

Emergence of Strong Exchange Interaction in the Actinide Series: The Driving Force for Magnetic Stabilization of Curium

K.T. Moore[1]*, G. van der Laan[2], R.G. Haire[3], M.A. Wall[1], A.J. Schwartz[1], P. Söderlind[1]

[1]*Lawrence Livermore National Laboratory, Livermore, California 94550, USA.*
[2]*Magnetic Spectroscopy Group, Daresbury Laboratory, Warrington WA4 4AD, UK.*
[3]*Oak Ridge National Laboratory, MS-6375, Oak Ridge, Tennessee 37831, USA.*

*Contact Author
Tel: 925-422-9741
Fax: 925-422-6892
Email: moore78@llnl.gov

Using electron energy-loss spectroscopy in a transmission electron microscope, many-electron atomic spectral calculations and density functional theory, we examine the electronic and magnetic structure of Cm metal. We show that angular momentum coupling in the 5*f* states plays a decisive role in the formation of the magnetic moment. The 5*f* states of Cm in intermediate coupling are strongly shifted towards the *LS* coupling limit due to exchange interaction, unlike most actinide elements where the effective spin-orbit interaction prevails. It is this *LS*-inclined intermediate coupling that is the key to producing the large spin polarization which in turn dictates the newly found crystal structure of Cm under pressure.

PACS: 79.20.Uv, 71.10.-w, 71.70.Ej, 71.70.Gm

Magnetic stabilization of crystal structures is rare and intriguing. In general, the driving force for magnetism is the exchange interaction that quantum-mechanically originates from the Pauli exclusion principle, in combination with electrostatic repulsion. In some metals, the magnetic interaction energy is sufficiently large to influence the crystal structure. Examples are manganese, iron and cobalt where appreciable exchange interaction creates a strong magnetic moment, which in turn dictates one or more crystallographic phases [1-3]. Recently, this list of metals with known magnetically stabilized crystal structures was extended to include a heavy actinide element.

During a contemporary surge in actinide condensed-matter physics [4-11] curium was found to have a phase induced by magnetism. In a diamond-anvil-cell study [12], Cm was pressurized up to ~100 GPa, causing the metal to undergo transformations between five different crystal structures, Cm I through Cm V. *Ab initio* calculations showed that the magnetic correlations in antiferromagnetic Cm play a crucial role in determining the crystal structures observed and that spin polarization of the 5*f* electrons is needed to achieve the correct sequence of phases during compression [12]. The calculations also showed that Cm III, which is monoclinic with the space group *C*2/*c*, could *not be stabilized* when spin polarization was neglected.

The 3*d* transition metals are an example where appreciable exchange interaction occurs, resulting in magnetism in some of the heavier metals in the series. However, the actinide metals exhibit a pronounced effective spin-orbit interaction of the 5*f* states due to strong relativistic effects, and this produces a considerable energy splitting and little mixing between the $5f_{5/2}$ and $5f_{7/2}$ levels [13]. Presently, there is no experimental evidence in the actinide series of the strong exchange interaction required to magnetically stabilize

a metallic phase. What mechanism then produces the strong spin polarization in Cm, which in turn is responsible for the formation of the Cm III phase?

Here, we investigate the electronic and magnetic structure of Cm using electron energy-loss spectroscopy (EELS) in a transmission electron microscope (TEM), many-electron atomic calculations and density functional theory. We show that for Cm the 5*f* states in intermediate coupling are strongly shifted towards the *LS* coupling limit, unlike most actinide metals that exhibit a strong effective spin-orbit interaction [13]. This *LS*–inclined intermediate coupling in Cm is due to exchange interaction, and is the mechanism responsible for producing the large spin polarization that magnetically stabilizes Cm III. Experimentally, we examine the room-pressure phase, Cm I, but the observed results are meaningful for Cm II and III as well. EELS experiments in the TEM [13], theoretical x-ray absorption spectra [14–16] and density-functional-theory (DFT) calculations [10,17] were performed in a similar manner to the references cited.

To date, absorption-type experiments have not been performed on Am or Cm, leaving their unoccupied electronic structure unmeasured. Here, the $N_{4,5}$ EELS spectra for Am and Cm metal are shown in Fig. 1(a). The Am spectra displays a strong N_5 ($4d_{5/2}\rightarrow 5f_{5/2,7/2}$) peak, but a very small N_4 ($4d_{3/2}\rightarrow 5f_{5/2}$) peak, while for Cm the N_5 and N_4 peaks are more equal in intensity. Using the experimentally measured branching ratio from the EELS spectra, atomic spectral calculations and sum-rule analysis, we can examine the transitions in detail. The branching ratio $B=I(N_5)/[I(N_5)+I(N_4)]$ was obtained as described in Refs. 15 and 16, where $I(N_5)$ and $I(N_4)$ are the integrated intensity of the N_5 and N_4 peaks, respectively. Sum-rule analysis was then performed using the experimental branching ratios, yielding the values of the spin-orbit interaction per hole.

For the *f* shell, the expectation value of the angular part of the spin-orbit parameter is $\langle w^{110} \rangle = 2/3 \langle l \cdot s \rangle = n_{7/2} - 4/3\ n_{5/2}$, where $n_{7/2}$ and $n_{5/2}$ are the electron occupation numbers for the angular-momentum levels $j = 7/2$ and 5/2 [15]. Thus, $\langle w^{110} \rangle$ reveals the proper angular momentum coupling scheme for a given material. For the $d \rightarrow f$ transition, the sum rule gives the spin-orbit interaction per hole as

$$\frac{\langle w^{110} \rangle}{14 - n_f} - \Delta = -\frac{5}{2}\left(B - \frac{3}{5}\right), \qquad (1)$$

where B is the measured branching ratio for the experimental EELS spectra, n_f is the number of electrons in the *f* shell, and Δ represents the small correction term for the sum rule that is calculated using Cowan's relativistic Hartree-Fock code [14].

The results of the spin-orbit analysis of the $N_{4,5}$ EELS spectra are plotted as blue points in Fig. 1(b). In addition to the present Am and Cm results, the results for Th, U and Pu from Ref. 16 are plotted for completeness. (Pu, Am and Cm values are given in Table I). The number of 5*f* electrons n_f for each metal is obtained from literature, where Th = 0.6, U = 3, Pu = 5, Am = 6 and Cm = 7 [18]. In addition to the EELS data, the results for *LS*, *jj* and intermediate coupling of the angular momenta, as given by atomic calculations, are plotted against the number of 5*f* electrons (n_f) as a short-dashed, long-dashed and solid line, respectively. Examining all the data in Fig. 1(b), it is clear that the 5*f* states of Am metal show an intermediate coupling mechanism that is close to the *jj* limit, meaning the majority of the six 5*f* electrons are in the j=5/2 manifold. The above sum rule results can in fact be understood directly from the Am EELS spectra in Fig. 1(a), since there is only a very small N_4 ($4d_{3/2}$) peak. Selection rules govern that a $d_{3/2}$ electron can only be excited into the $f_{5/2}$ level, and since the $f_{5/2}$ is almost full, being only able to holds six

electrons, there is almost no transition. The branching ratio and sum-rule analysis of Cm show it too exhibits an intermediate coupling mechanism, but in this case it is much closer to the *LS* limit, as illustrated in Fig. 1(b). This results in a larger intensity of the N_4 peak, relative to the N_5 peak, in the EELS spectrum, as seen in Fig. 1(a).

The abrupt and striking change in the behavior of the 5*f* electrons at Cm is caused by exchange interaction. *jj* coupling prefers all the electrons to be in the $f_{5/2}$ level, which can hold no more than six. The maximal energy gain in *jj* coupling is thus obtained for Am f^6, since the $f_{5/2}$ level is filled. However, for Cm f^7 at least one electron will be relegated to the $f_{7/2}$ level. The f^7 configuration has the maximal energy stabilization due to the exchange interaction, with all spins parallel in the half filled shell, and this can only be achieved in *LS* coupling. Thus, the large changes observed in the electronic and magnetic properties of the actinides at Cm are due to this transition from optimal spin-orbit stabilization for f^6 to optimal exchange interaction stabilization for f^7. In all cases the spin-orbit and exchange interaction compete with each other, resulting in intermediate coupling; however, increasing the *f* count from 6 to 7 shows a clear and pronounced shift in the power balance in favor of the exchange interaction. In fact, the effect is so strong that, compared to Am, not one but two electrons are transferred to the $f_{7/2}$ level in Cm (c.f. Table I).

The spin and orbital magnetic moments from atomic calculations are plotted against n_f in Fig. 2(a) and (b), respectively. In each graph, the three different angular momentum coupling mechanisms are shown: *LS*, *jj* and intermediate. Examining the plots, we see that for some elements the choice of coupling mechanism has a large influence on the spin and orbital moments. This is most remarkable for Cm (n_f = 7),

where Fig. 2(a) shows that the spin moment is modest for the *jj* coupling limit, but is large for both *LS* and intermediate coupling. The fact that the spin moment for the intermediate coupling is almost as large as that for the *LS* limit is because the intermediate coupling curve moves strongly back towards the *LS* limit at Cm in Fig. 1(b). Thus, it is the pronounced shift of the intermediate coupling curve towards the *LS* coupling limit at Cm – in order to accommodate the exchange interaction – that creates a large and abrupt change in the electron occupancy of the $f_{5/2}$ and $f_{7/2}$ levels shown in Fig. 2(c). In this figure, the $n_{5/2}$ and $n_{7/2}$ occupation numbers are shown for atomic calculations in intermediate coupling by the black and red lines, respectively, and for the spin-orbit analysis of the experimental EELS spectra as blue points. If the intermediate coupling curve remained near the *jj* limit for Cm, the spin (and total) moment would be much smaller than the observed 7 μ_B/atom [19] magnetic moment and have little or no effect on the crystal structure of the metal.

In order to further examine the topic of spin polarization and phase stability, we performed DFT calculations for each of the five polymorphic phases of Cm (I – V) for both spin-polarized and non-magnetic configurations. The total energies of each phase are plotted as a function of volume in Fig. 3. One conclusion is that spin polarization is needed to capture the correct order of phases, as previously shown [12]. What else is clear from Fig. 3 is that the non-magnetic calculations are much higher in energy than the spin-polarized calculations and that the energy difference between the spin-polarized and non-magnetic calculations for Cm I, II and III is large, but becomes smaller for Cm IV and V as the volume is decreased. This means that the spin polarization is strong for the lower-pressure phases, but then diminishes, becoming less important for the high-

pressure phases. As the volume is decreased, the 5*f* wave functions overlap increase, leading to broader bands that lessen the preference for spin polarization with reduced magnetism as a consequence. Indeed, examining at the spin, orbital and total magnetic moments in Table II, it can be seen that the moments steadily decrease with pressure, abruptly disappearing at Cm V.

The topic of magnetism in the actinides is strongly debated, particularly in plutonium [10,20], where to date there has been no convincing experimental evidence for significant moments in any of the six allotropic metal phases. This is a conundrum given the fact that Pu is f^5 with one hole in the $f_{5/2}$ level [13]. Why is Cm magnetic, but Pu is not? Pu (f^5) and Cm (f^7) both have roughly the same amount of $f_{5/2}$ electrons, but while Pu has 0.67 $f_{7/2}$ electrons, Cm has 2.59 (c.f. Table I). The angular moment coupling of the five 5*f* electrons in Pu are governed by the strong spin-orbit interaction, resulting in a spin that is rigidly coupled antiparallel to its orbital moment. Figure 2(a) and (b) shows that for Pu the spin and orbital magnetic moments are opposite and almost equal. This has been known for some time, and has also been suggested by DFT [10], but may not be the entire answer of why there is an apparent lack of significant magnetic moments in Pu. Recent magnetic susceptibility measurements have shown that localized magnetic moments do indeed form in plutonium as damage accumulates due to self-irradiation [21]. The quest to understand the magnetic behavior of Pu continues. In the case of Cm, however, the seven 5*f* electrons forming a half-filled shell are stabilized by exchange interaction, resulting in a large spin moment in both intermediate and *LS* coupling. This is a situation resembling that of Gd f^7, which has the highest Curie temperature amongst the rare earth elements and a large magnetic moment. Cm also has a modest orbital

moment that is parallel to the large spin moment, as shown in Fig. 2 (a) and (b), due to the non-vanishing spin-orbit interaction in intermediate coupling. Thus, it is clear why Cm is strongly magnetic, and here we see that the electron coupling mechanism plays a dominant role, being the root cause for the magnetic stabilization of curium. These results also illustrate that strong exchange interaction is an integral part of magnetic stabilization of a metal, whether it is Fe, Mn, Co, or even the heavy actinide Cm.

This work was performed under the auspices of U.S. Department of Energy by the University of California, Lawrence Livermore National Laboratory under Contract No. W-7405-Eng-48 and by DE-AC05-00OR22725 with ORNL, operated by UT-Battelle.

References

[1] P. Söderlind *et al.*, *Nature* **374**, 524 (1995).
[2] O. K. Andersen *et al.*, *Phys. B* **86-88**, 249 (1977).
[3] P. Söderlind *et al.*, *Phys. Rev. B* **50**, 5918 (1994).
[4] S. Y. Savrasov, G. Kotliar, and E. Abrahams, *Nature* **410**, 793 (2001).
[5] L. Havela *et al.*, *Phys. Rev. B* **65**, 235118 (2002).
[6] J. L. Sarrao *et al.*, *Nature* **420**, 297 (2002).
[7] G.H. Lander, *Science* **301**, 1057 (2003).
[8] J. Wong *et al.*, *Science* **301**, 1078 (2003).
[9] X. Dai *et al.*, *Science* **300**, 953 (2003).
[10] P. Söderlind, B. Sadigh, *Phys. Rev. Lett* **92**, 185702 (2004).
[11] K.T. Moore *et al.*, *Phys. Rev. Lett* **96**, 206402 (2006).
[12] S. Heathman *et al.*, *Science* **309**, 110 (2005).
[13] K.T. Moore *et al.*, *Phys. Rev. Lett.* **90**, 196404 (2003); K. T. Moore *et al.*, *Phil. Mag.* **84**, 1039 (2004); K. T. Moore *et al.*, *Phys. Rev. B* **73**, 033109 (2006).
[14] R. D. Cowan, *The Theory of Atomic Structure and Spectra* (University of California Press, Berkeley, 1981).
[15] G. van der Laan and B. T. Thole, *Phys. Rev. B* **53**, 14458 (1996).
[16] G. van der Laan *et al.*, *Phys. Rev. Lett.* **93,** 097401 (2004).
[17] P. Söderlind and A. Landa, *Phys. Rev. B* **72,** 024109 (2005).
[18] A.J. Freeman and G.H. Lander, Ed., *Handbook on the Physics and Chemistry of the Actinides* (Elsevier Science Ltd., Amsterdam, 1984).
[19] P.G. Huray *et al.*, *Physica B+C* **102B**, 217 (1980); S.E. Nave, R.G. Haire and P.G. Huray *Phys. Rev. B* **28,** 2317 (1983).
[20] J.C. Lashley *et al., Phys. Rev. B* **72**, 045135 (2005).
[21] S.K. McCall *et al.*, *Proc. Natl. Acad. Sci. USA* **103**, 17179 (2006).

Table I: The number of f electrons (n_f), the measured branching ratio, B, of the $N_{4,5}$ EELS spectra and the expectation value of the 5f spin-orbit interaction per hole, $\langle w^{110} \rangle/(14-n_f)$, obtained using Eq. (1) for Pu (Ref. 16), Am and Cm metal (current work). The sum rule requires a small correction factor, which is $\Delta = 0$, 0.005 and 0.015 for $n = 5$, 6 and 7, respectively. The electron occupation numbers of the $f_{5/2}$ and $f_{7/2}$ levels obtained by solving $\langle w^{110} \rangle = n_{7/2} - 4/3\ n_{5/2}$ and $n_f = n_{7/2} + n_{5/2}$.

Metal	n_f	Branching ratio (B)	$\langle w^{110} \rangle/(14-n_f)-\Delta$	$n_{5/2}$	$n_{7/2}$
Pu	5	0.826 (010)	-0.565 (025)	4.32	0.67
Am	6	0.930 (005)	-0.830 (013)	5.38	0.62
Cm	7	0.794 (003)	-0.485 (008)	4.41	2.59

Table II: The spin, orbital and total moments for Cm I – V as calculated by DFT.

Cm phase	Volume (Å^3)	Spin moment (μ_B)	Orbital moment (μ_B)	Total moment (μ_B)
I	30	6.6	0.4	7.0
II	22.8	6.16	0.35	6.51
III	18.9	5.43	0.38	5.81
IV	16.7	4.57	0.59	5.16
V	13.7	0	0	0

Figure captions

Fig. 1: (a) The $N_{4,5}$ EELS spectra of Am and Cm metal acquired in a TEM. (b) A plot of $<w^{110}>/(14-n) - \Delta$ as a function of the number of 5*f* electrons (n_f). The three theoretical angular momentum coupling schemes are shown: *LS*, *jj*, and intermediate. Data from the experimentally measured branching ratios of each metal are indicated by blue points. Note the large shift of the intermediate coupling curve towards the *LS* limit at $n_f = 7$.

Fig. 2: The atomic (a) spin and (b) orbital magnetic moment for the actinide elements against the number of 5*f* electrons (n_f). The three theoretical angular momentum coupling schemes are shown in each plot: *LS*, *jj*, and intermediate coupling. The spin moment is large and positive for Cm for either the intermediate or *LS* coupling scheme, but considerably smaller for the *jj* limit. Since Cm exhibits intermediate coupling, this is the key to producing the large magnetic moment that strongly influences the crystal structure of the metal. (c) The electron occupation numbers $n_{5/2}$ (solid black line) and $n_{7/2}$ (solid red line) in intermediate coupling as a function of n_f. . The $n_{5/2}$ and $n_{7/2}$ occupation numbers from the spin-orbit analysis of the EELS spectra are indicated by blue points. Note the large discontinuity in these numbers that occurs at Cm, breaking the gradual change across the lighter actinides.

Fig. 3: Calculated total energies for the five polymorphic phases of Cm (I – V) as a function of atomic volume for both spin polarized and non-magnetic configurations. The vertical black lines indicate the experimentally measured phase transition volumes [12].

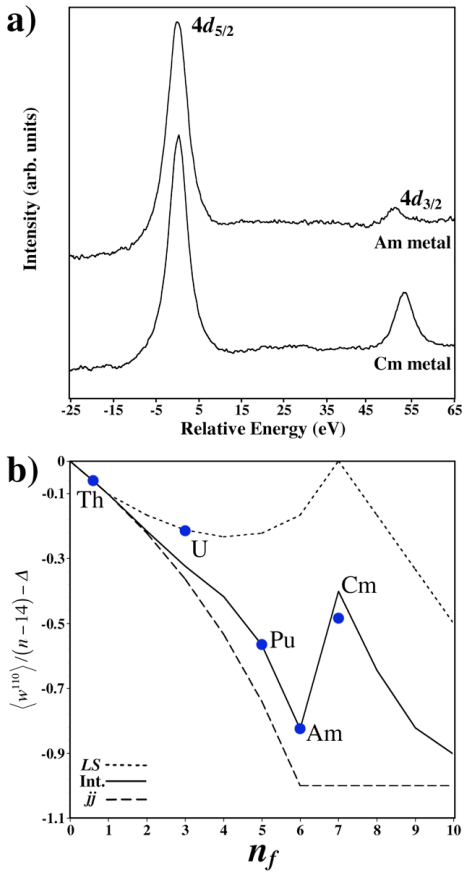
a)
$4d_{5/2}$
$4d_{3/2}$
Am metal
Cm metal
Intensity (arb. units)
-25 -15 -5 5 15 25 35 45 55 65
Relative Energy (eV)
b)
Th
U
Cm
Pu
Am
LS
Int.
jj
$\langle w^{(10)} \rangle / (n-14) - \Delta$
0 -0.1 -0.3 -0.5 -0.7 -0.9 -1.1
0 1 2 3 4 5 6 7 8 9 10
n_f

Fig. 1

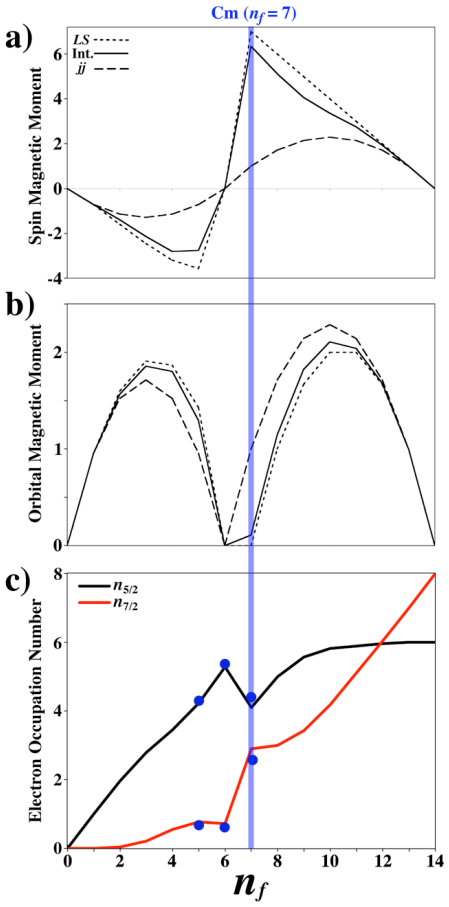
Cm (n_f = 7)
a)
LS
Int.
jj
Spin Magnetic Moment
b)
Orbital Magnetic Moment
c)
$n_{5/2}$
$n_{7/2}$
Electron Occupation Number
n_f

Fig. 2

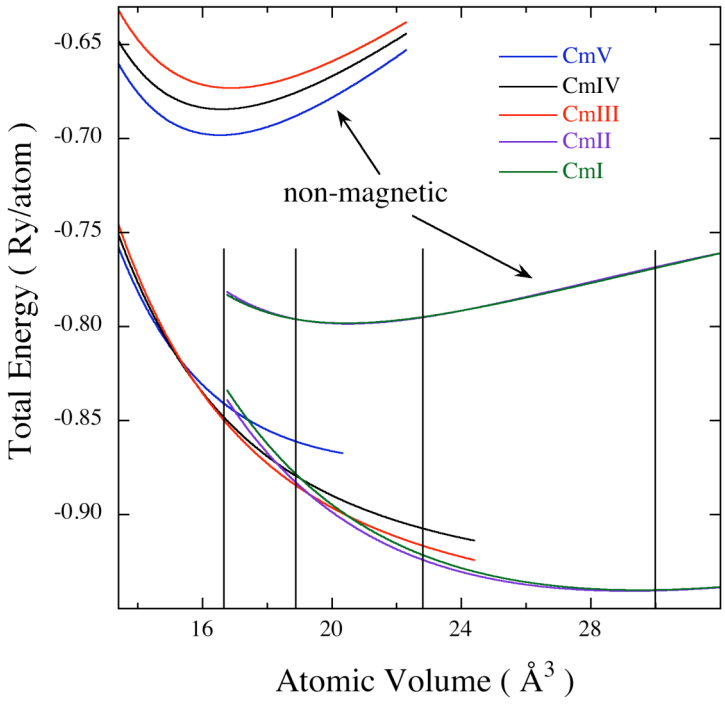
-0.65
-0.70
-0.75
-0.80
-0.85
-0.90
Total Energy (Ry/atom)
16
20
24
28
Atomic Volume (Å^3)
CmV
CmIV
CmIII
CmII
CmI
non-magnetic

Fig. 3